

THE EFFECT OF Al CONTENT ON HYDROGEN ABSORPTION AND MECHANICAL PROPERTIES OF FeAl PHASE

ABSTRACT

The influence of the aluminium content in the FeAl phase on the absorption of hydrogen generating spontaneously or electrolytically from the surrounding environment, was determined. The ability of the FeAl phase to absorb hydrogen was examined in terms of the hydrogen content changes of the effective diffusion coefficient, and the results of the three-point bending as well as the hardness measurements.

Key words: Hydrogen permeability, Iron aluminide, FeAl, B2 type intermetallic alloys.

INTRODUCTION

The plasticity of iron or nickel aluminides drastically decreases in the environment enable to produce hydrogen [1-13]. Hydrogen formed on the sample surface, due to the chemical reaction between moisture and aluminium, causes a decrease in ductility. This phenomenon is called environmental embrittlement. The presence of notches on the alloy surface facilitates the penetration of hydrogen into the alloy. The amount of hydrogen penetrating into the iron aluminide depends on the condition of the alumina surface layer, on the exposure time, and on the rate of hydrogen diffusion [9-12].

In the present studies an attempt was made to determine the relationship between the composition of the binary FeAl alloys and their tendency to absorb hydrogen from air and during an electrolytic saturation.

EXPERIMENTAL PROCEDURE

Studies were carried out on the single-phase binary Fe-Al alloys of composition shown in Table 1. The alloys were produced from ARMCO iron and they metallic aluminium, and they were remelted three times in a laboratory induction furnace. Graphite crucibles were used for ingot casting [13].

The ingots of 20 and 6 mm in diameter and 70 mm in length were cast and their concave tops were cut off. Then, they were homogenized at 1273K for 72h followed by furnace cooling. A part of the homogenized ingots was additionally annealed at 673K for 120h in order to eliminate thermal vacancies. The electrical resistance of the all studied alloys was measured.

Samples of 5 mm length were cut from the 6 mm diameter ingots. The sample surface was cleaned by dry grinding. A part of the samples was subjected to hydrogen absorption in air while the other part was electrolytically saturated. The hydrogen concentration was determined by means of the STRÖHLEIN INSTRUMENTS H-MAT 2500 analyzer.

Table 1. Chemical composition of the studied FeAl alloys

Alloy	Element content [wt. %]							
	Al	Si	Mn	C	S	P	Fe	O[ppm]
Fe37Al	22.18	0.11	0.019	0.013	0.008	0.019	77.70	117
Fe40Al	24.18	0.19	0.015	0.046	0.006	0.055	75.19	70
Fe43Al	26.89	0.21	0.034	0.037	0.005	0.025	73.09	43
Fe46Al	29.19	0.15	0.029	0.014	0.003	0.022	70.75	56
Fe50Al	32.61	0.03	0.026	0.018	0.005	0.016	67.39	37

The other samples, in the form of 3 mm thick membranes were cut from the 20 mm ingots. They were properly cleaned by grinding and polishing and then, they were etched in a concentrated solution of HCl. The output side of the membranes was coated with palladium in order to isolate the metal surface from the NaOH solution and to increase the hydrogen ionization rate. In the process of the palladium coating the membrane served as the cathode. An aquorus solution of $0.8 \text{ gdm}^{-3} \text{ PdCl}_2 + 60 \text{ gdm}^{-3} \text{ NaOH}$, was used for this process and a catodic current density of 200 Am^{-2} for the first 30 s, and of 100 Am^{-2} for the next 270s was applied.

Hydrogen will penetrate into the FeAl alloy when its surface layer of alumina is destroyed. This can be done by a proper choice of the electrolyte that will chemically destroy the layer at the input surface of the membrane, but it will not or only weakly interact with the membrane itself. After some experiments [15], the water 35% NaCl solution was chosen. The hydrogen penetration through the membranes was measured using the electrochemical Devanathan and Stachurski method [14]. The curves of the permeation current versus time of hydrogen saturation were determined for the applied cothodic current density of 0.013 A/m^2 at the membrane input side. The measurements were carried out at room temperature.

The permeation of hydrogen through the membranes was illustrated by the curves of the permeation current (i_p) versus saturation time (Fig. 1). The so called time delay (t_L) can be determind as the time corresponding to the ratio [14]:

$$\frac{i_p}{i_{p.\max}} = 0,617 \quad (1)$$

where $i_{p.\max}$ is a steady state (maximum) permeation rate. The t_L may be used for calculating the diffusion coefficient of hydrogen:

$$D = \frac{L^2}{6t_L} \quad (2)$$

where L is the membrane thickness.

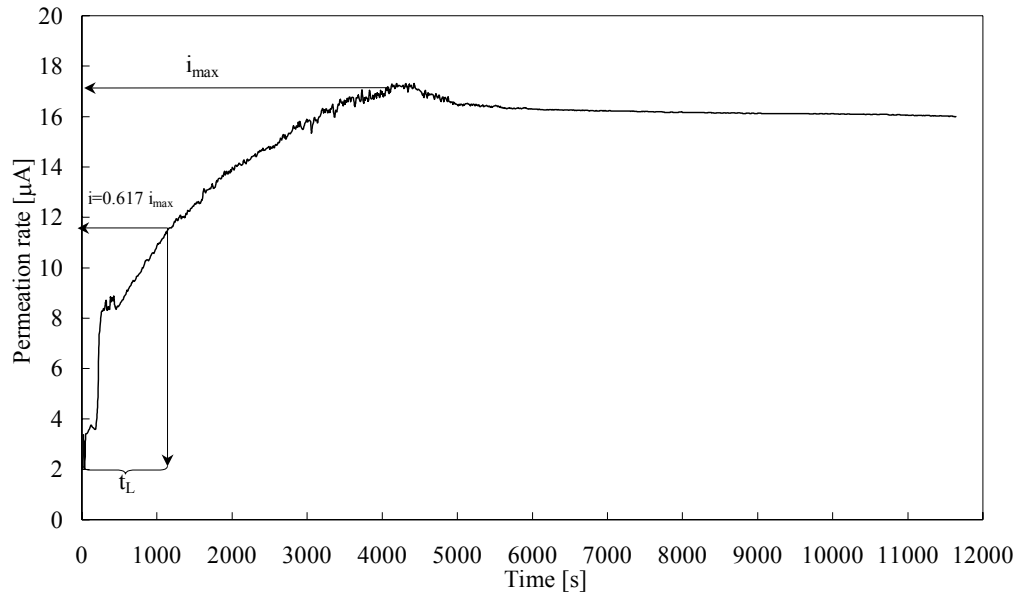


Fig. 1. Experimental permeation rate – time curve for FeAl membranes and an evolution of the time t_L

The annealed membranes were polished and then etched in a solution containing: 33% HNO_3 + 33% CH_3COOH + 8% HF + 26% H_2O . Microstructures were observed and the grain sizes were measured using the light microscope NEOPHOT 2. Also X-ray phase analysis was carried out using a Philips diffractometer with CuK_α radiation, and the long-range order parameter was determined.

The three-point bending tests were carried out for the specimens annealed and hydrogen saturated at room temperature in the argon atmosphere using the INSTRON 1195 testing machine. The cross-head speed was 0.1mm/min and the deflection versus the bending force P was recorded.

Microhardness was measured using a Vickers testing machine with 1.6 kN load. The loading time was 15 s.

EXPERIMENTAL RESULTS

The defect concentration indicator, measured with the use of the electron resistance meter [16], had the same dependence on aluminum content for the homogenized samples and for the homogenized and then annealed samples (Fig. 2).

These results show that cooling with the furnace leads to the equilibrium density of defects in the alloy structure and that the additional annealing at 673K for 120 hours does not change defect concentration. The increase in the defect density for the non-stoichiometric alloys is related to the formation of antisite defects. If we assume the defect density for the stoichiometric (equi-atomic) FeAl alloy as the equilibrium for 673K, then the observed increase of the defect density indicator for non-stoichiometric alloys is caused by the aluminum deficiency.

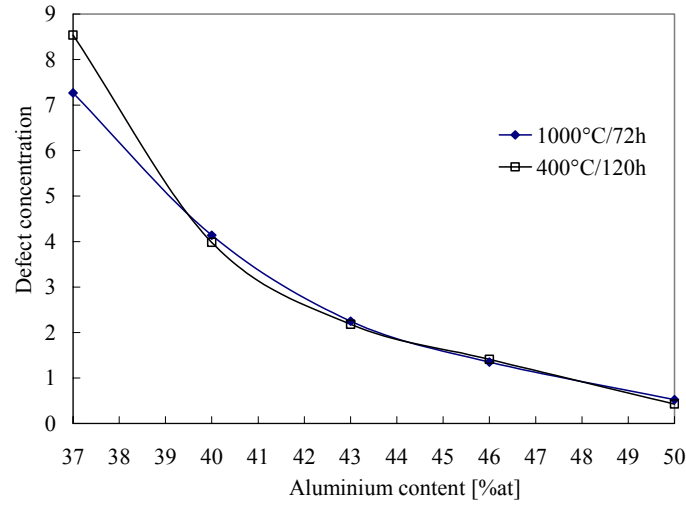


Fig. 2. Indicator of defect concentration plotted versus aluminium content in FeAl alloys

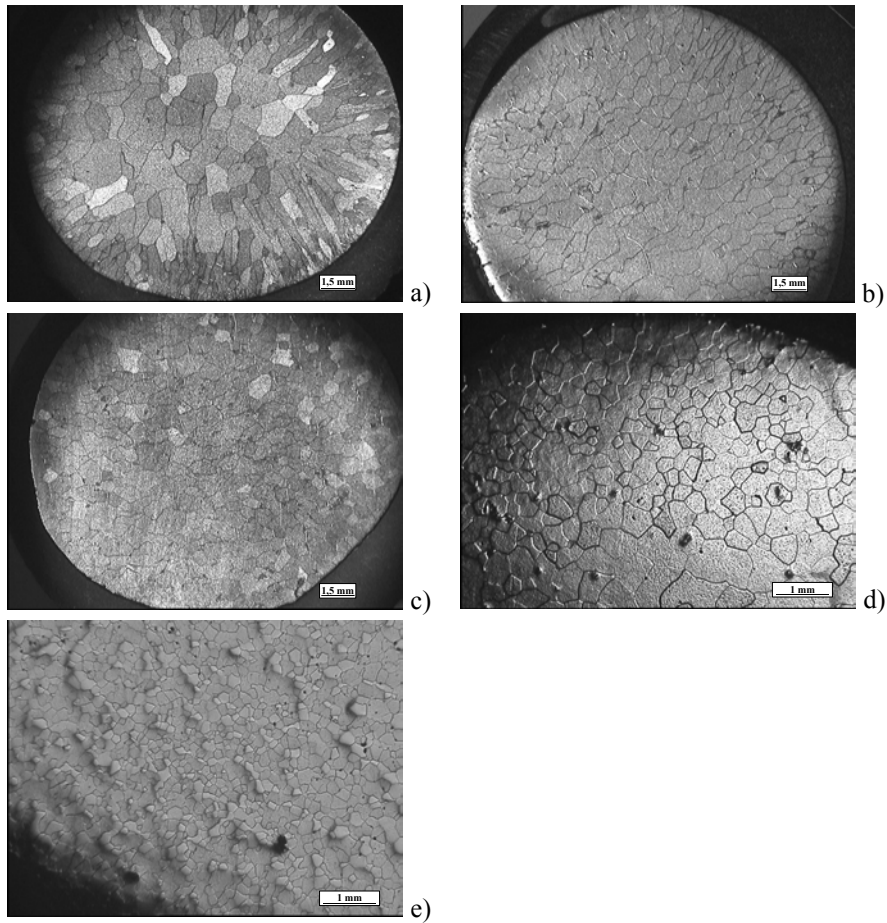


Fig. 3. Microstructure of intermetallics: a – 37 % Al; b – 40% Al; c – 43 % Al; d – 46 % Al; e – 50% Al (%at.)

Due to this tendency to form the antisite defects, the FeAl alloys maintain a stable B2 structure within a large range of the alloy composition (from 36 at. % to 50.5 at. %). The deficiency of aluminum in the binary FeAl is reflected in the alloy microstructure (Fig. 3). The alloys containing from 46 at.% of Al up to stoichiometric composition have smaller equized grains. When the content of iron in the alloy increases, the grain sizes are larger and they show dendrite morphology. Between the dendrites arms at the grain boundaries, the pores generated during the crystallization can be visible. The comparison of the structure changes with the defect indicator (Fig. 2) leads to the conclusion that stabilization of the B2 crystal structure is due to creation of the point defects. An increase in the defect density causes an increase in the grain sizes (Fig. 4).

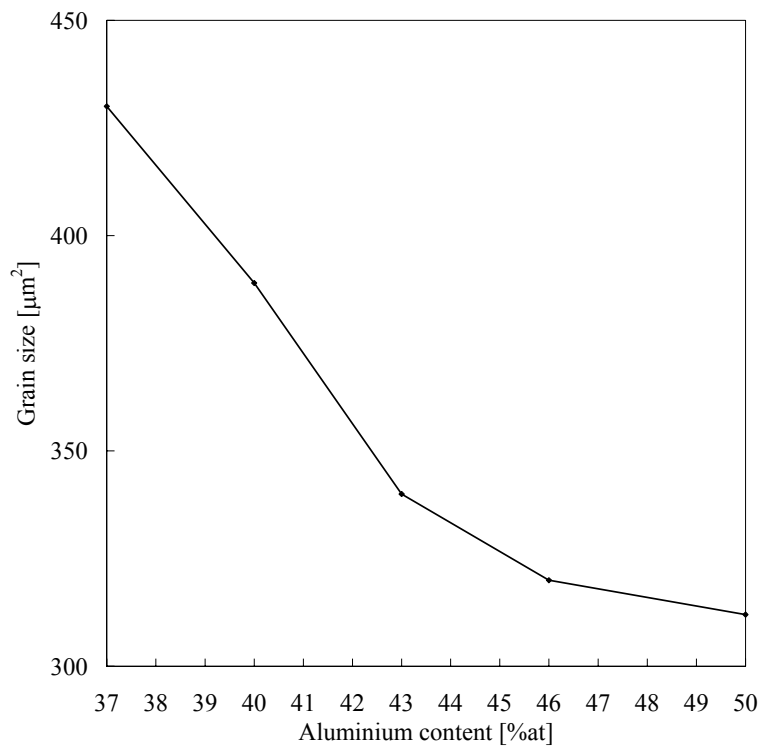


Fig. 4. Grain size of FeAl phase against aluminium content for FeAl phase

During the preparation of samples from the 6-mm diameter ingots (cutting off the sinkheads, polishing) they absorb significant amount of hydrogen from air (Fig. 5). Concentration of hydrogen absorbed in sub-stoichiometric alloys changes almost linearly with aluminum content. A larger increase of the hydrogen concentration occurs in the stoichiometric alloy. In order to check the stability of the hydrogen “building” in the structure, the Fe40Al and Fe50Al alloys, the samples were to annealed at 1073 K for 2 hours. The annealing was carried out in a vacuum furnace under pressure of 10^{-5} Pa, and then, the samples were cooled down with the furnace. After reaching room temperature, the samples were removed from the furnace and kept in liquid nitrogen until the measurement of hydrogen content. The measured hydrogen concentrations were 0.073 ppm and 0.62 ppm for the Fe40Al and Fe50Al alloys, respectively (the values are indicated in Fig. 5 as dots). As seen, hydrogen almost completely desorbed from the sub-stoichiometric alloys but a quite large hydrogen concentration was in the equiatomic

FeAl phase. The difference in the hydrogen desorption in alloys of different aluminum content is probably related to different alloy structures. The sub-stoichiometric alloys show dendrite coarse grains while the stoichiometric alloy exhibits fine izomorphic grain structure.

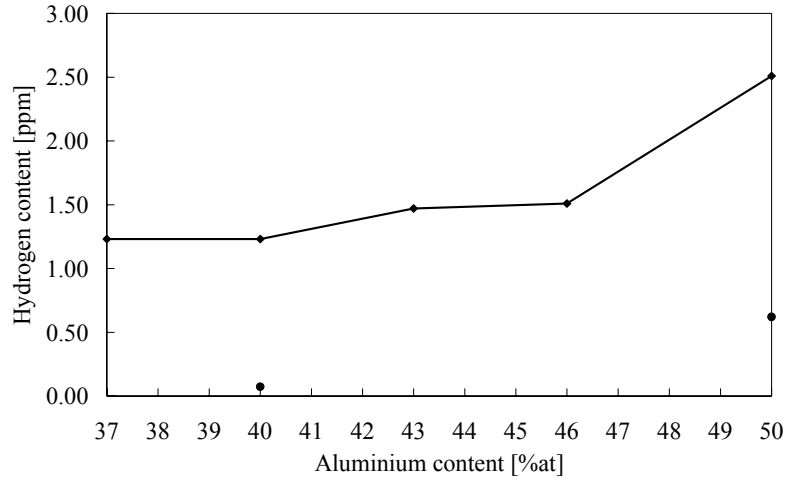


Fig. 5. Initial (prior to H saturation) content of hydrogen in FeAl phase versus aluminium content

Plasticity of the FeAl phase decreases with the aluminum content increase (Fig. 6, curve a). The stoichiometric alloy containing the highest amount of hydrogen absorbed from the air show the highest brittleness. This alloy also shows the largest parameter of long range order (Fig. 7). The values of the structure parameters and properties of the alloys before cathodic saturation are shown in Table 2.

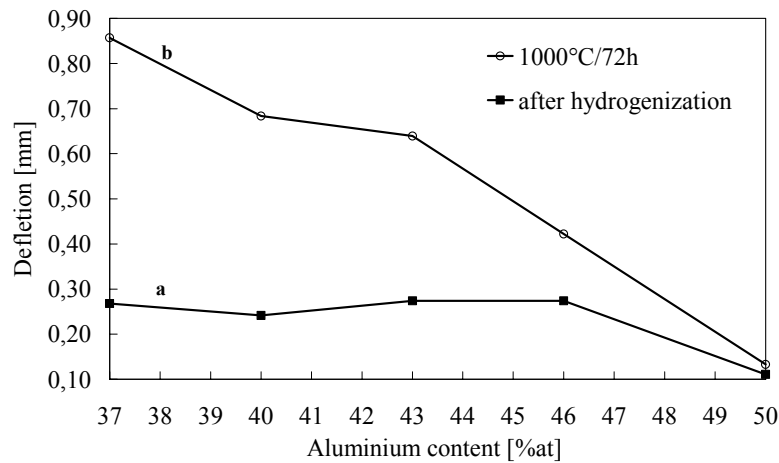
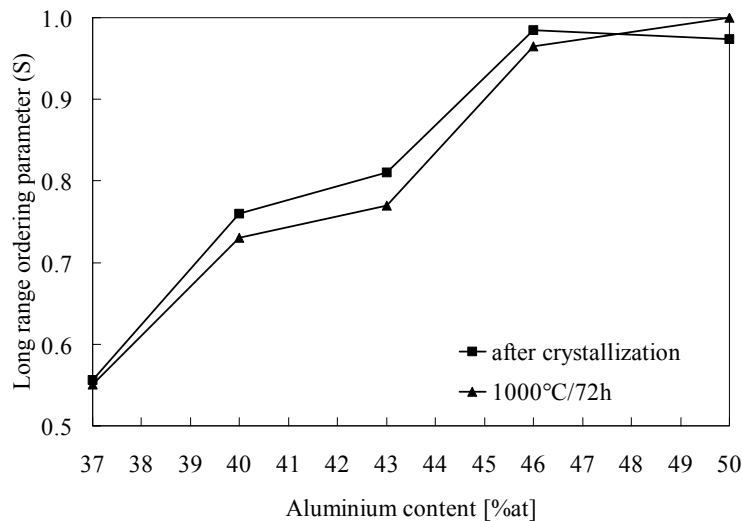


Fig. 6. Deflection of sample at fracture in bending before (a) and after saturation with hydrogen (b) versus aluminium content

Table 2. Structure parameters and properties of the FeAl phase before hydrogen saturation versus aluminum content

Measured value	Aluminum concentration [%at.]				
	37	40	43	46	50
Grain size [μm]	430	389	340	320	312
Long-range parameter	0.55	0.73	0.8	0.97	1
Vacancy concentration indicator	7.27	4.14	2.25	1.35	0.53
Deflection f [mm]	0.86	0.68	0.64	0.42	0.13
Bending strength [MPa]	763	664	657	708	254
Microhardness [μHV]	308	341	413	457	499

**Fig. 7.** Relationships between long-range ordering parameter (S) and aluminium content

The hydrogen saturation was applied to both the membranes and the rods of 5 mm diameter and 6 mm length. The samples were saturated at the same current–voltage conditions but taking into account their different shape and sizes. Hydrogen charged rods were used to determine the hydrogen concentration versus the aluminum content in the FeAl alloy (Fig. 8). Similarly as in the case of spontaneous hydrogen absorption from the air its concentration after the cathodic saturation reaches the highest value for the equi-atomic alloy. The diffusion coefficient, obtained from the $i_p = f(t)$ curves, decreases with increase of aluminum concentration (Fig. 9). The lowest value of this coefficient is for the equi-atomic alloy, i.e. for that which has also the highest ability to hydrogen absorption both from air and during the cathodic saturation. The effective diffusion coefficient reaches the highest value for the Fe37Al alloy. Changes in the diffusion coefficient versus the aluminum content are smaller than 1 order of magnitude.

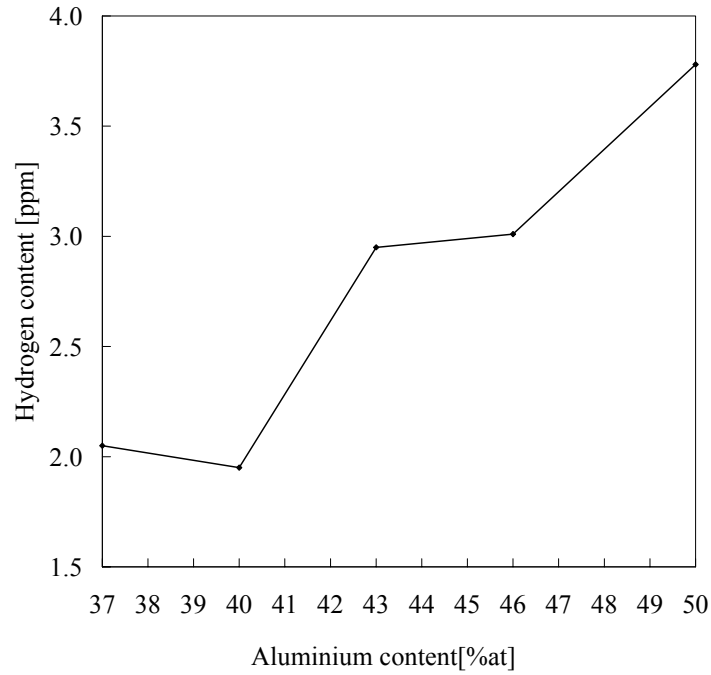


Fig. 8. Hydrogen content in FeAl phase versus aluminium content for samples cathodically charged for 10 hours

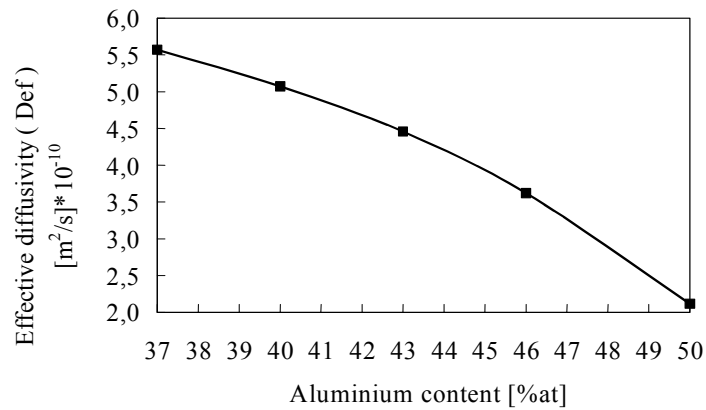


Fig. 9. Effective diffusion coefficient plotted versus aluminium content in FeAl phase

The hardness of the FeAl phase after its cathode charging was higher in all the alloys (Fig. 10). Both curves shown in Fig. 10 have almost the same trend. Differences in microhardness before and after charging decrease with increasing aluminium content (Fig. 11). This increase in the microhardness (Fig. 11) is similar to the changes of grain sizes (Fig. 4) and the point defect indicator (Fig. 2). Similarly, the difference in the deflection at rupture during bend testing, before and after hydrogen charging (Fig. 6), decreases with the increasing aluminium content.

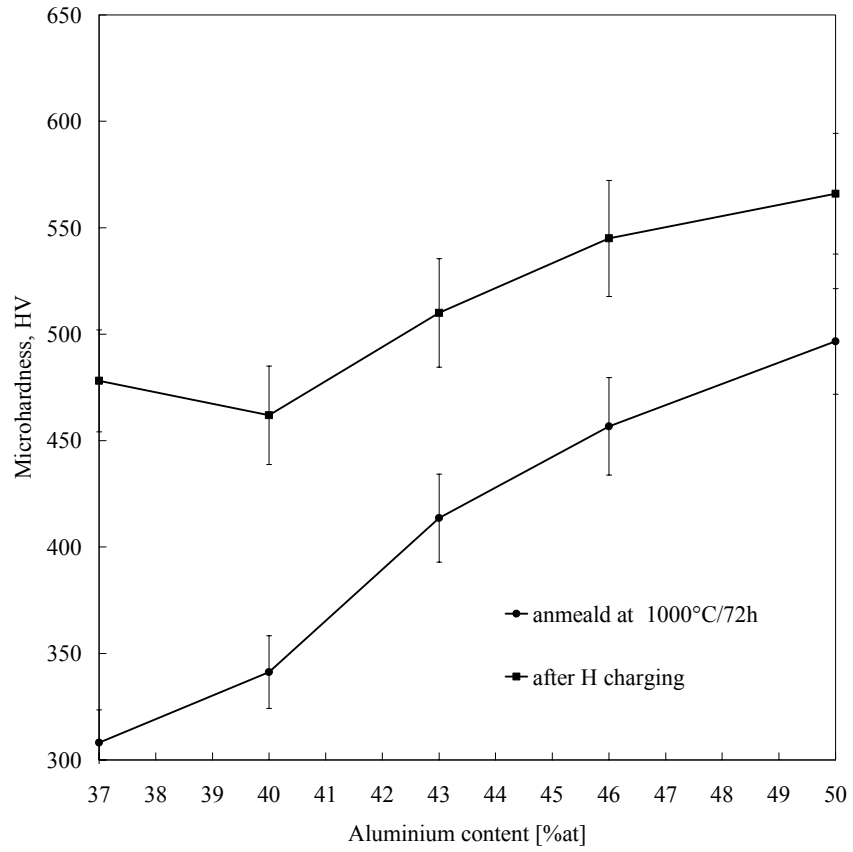


Fig. 10. Microhardness of FeAl phase before and after saturation with hydrogen versus aluminium content

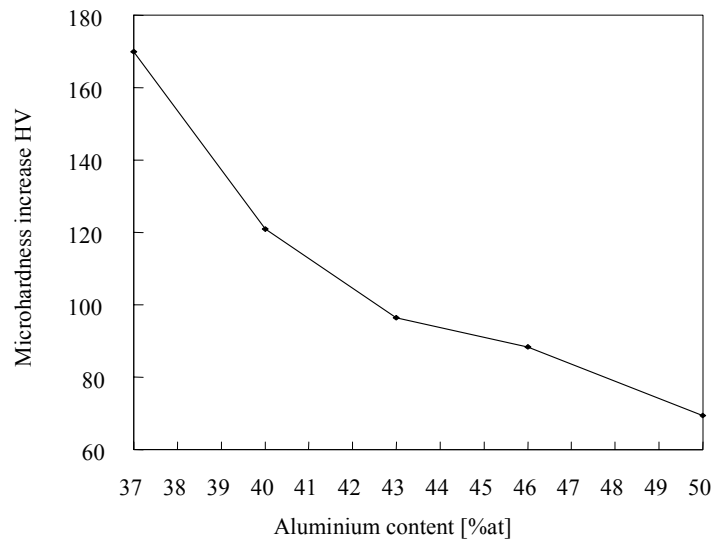


Fig. 11. Increase of microhardness of FeAl phase caused by its saturation with hydrogen versus aluminium content

DISCUSSION

The two-component alloys of the intermetallic FeAl phase show high susceptibility to hydrogen absorption independently of aluminum concentration. Removing the alumina layer during the sample preparation enables hydrogen penetration into the alloy. The amount of the absorbed hydrogen very weakly depends on the alloy composition (Fig. 5) for the under-stoichiometric alloys exhibiting dendritic large grain structure (Figs. 2, 3). But it significantly increases for the equi-atomic phase that shows equiaxed fine grains. This suggests that the susceptibility to hydrogen saturation depends mainly on the alloy structure and less on the aluminum content. The highly defected structure of the under-stoichiometric alloys is a „sieve” for absorbing hydrogen, while the compact structure of the stoichiometric phase shows tendency for hydrogen trapping. This is confirmed by the variation of the diffusion coefficient versus aluminum concentration (Fig. 9). For under-stoichiometric alloys this coefficient changes linearly while for the equi-atomic FeAl phase it decreases faster. Also the measurements of desorption of hydrogen during annealing (Fig. 5) show that it is more difficult to remove hydrogen from the stoichiometric alloy than from the under-stoichiometric Fe40Al. Thus, hydrogen trapping depends on the alloy stoichiometry.

The effective diffusion coefficient, determined for the studied FeAl alloy using the Devanathan – Stachurski method, changes in the range of one order of magnitude from $5.6 \cdot 10^{-10}$ m²/s for Fe37Al (at.%) to $2.10 \cdot 10^{-10}$ m²/s for the equi-atomic alloy. It seems that the determined values of the diffusion coefficient of hydrogen in the Fe-Al phase are correct, taking into account discrepancies of these measurements shown in literature data. The values of the effective diffusion coefficient determined in [17] for the Fe28Al5Cr0.5Mo0.2Co0.2Br0.1Zr alloy is $D_{\text{ef}} \approx 1.6 \cdot 10^{-9}$ m²/s, for the two-component Fe18Al alloy $D_{\text{ef}} \approx 10^{-11}$ m²/s, and for the Fe25Al alloy $D_{\text{ef}} = 4.4 \cdot 10^{-13}$ m²/s [18], while for the Fe40Al alloy $D \approx 10^{-13}$ m²/s [19]. If we take into account differences in the alloy composition, we can claim that the values determined in this work are correct.

The concentration of hydrogen absorbed during cathode saturation versus the aluminum content in the alloy (Fig. 8) has a similar variation as in case of hydrogen absorption from air (Fig. 5). The smallest hydrogen concentration was found in the Fe37Al and the largest – in the stoichiometric FeAl phase. However, for the under-stoichiometric alloys there is no linear dependence between the absorbed hydrogen and the aluminum content. The observed differences in hydrogen absorbed by cathode saturation are most probably due to different hydrogen sources and conditions of its absorption. Hydrogen absorption from air occurs on the whole sample surface after removing the protecting alumina layer. This suggestion is confirmed by the results of the authors of [20, 21], who claimed that during saturation in air hydrogen penetrates the material only 0.09 mm deep. However, during cathode saturation hydrogen penetrates through the whole membrane thickness and there exists different conditions for hydrogen trapping.

The concentration of hydrogen during in the FeAl phase of different aluminum content shows some relation to the degree of the long-range order (compare Fig. 7 and 8). The alloys with higher degree of order show higher ability of hydrogen trapping. This is confirmed by the results of [22], where it was found that the (CoFe)₃V alloy of high long-range order showed susceptibility to increased environmental embrittlement caused by humid air, while the disordered alloys were more resistant. The differences in alloy susceptibility were explained in terms of thermodynamic relations and hydrogen transport

The present results show that equi-atomic alloys of long-range order parameter close to one exhibit much higher ability of hydrogen trapping than the non-stoichiometric alloys.

The susceptibility to hydrogen trapping by the equi-atomic FeAl phase, that is from its nature very brittle, does not show significant environmental embrittlement. The decrease in plasticity is clearly visible in the alloys of large deviation from stoichiometry (Fe-Al 37-43 %at.Al).

CONCLUSIONS

1. Intermetallic FeAl alloys of different concentration of aluminium absorb hydrogen from the humid air. The higher degree of the alloy long-range order, the higher amount of the absorbed hydrogen.
2. Alloys with smaller equized grains exhibit higher ability to hydrogen absorption than the alloys with large dendritic grain structure, i.e. with large density of defects.
3. The effective diffusivity of hydrogen decreases with the decreasing content of aluminium. This decrease is within the range of one order of magnitude. The effective diffusivity of hydrogen versus aluminum content shows the "opposite" relation as compared to the defect concentration indicator.

REFERENCES

1. Liu C.T., George E., *Scr. Metall.* **24**, (1990) 875.
2. Stoloff N.S., Liu C.T., *Intermetallics*, **2**, (1994), 75.
3. Lynch R.J., Harburn H., Macione L., Heldt L.A., *Scripta Metall. et Materialia* **30**, (1994), 1157.
4. Liu C.T., George E.A., Maziarz P.J., Schneibel J.H., *Mater. Sci. Eng. A* **258**, (1998), 84.
5. Makamura M., Kamugai T., *Metall. and Mater. Trans.* **30A**, (1999), 3089.
6. Zhu Y.F., Liu C.T., Chen C.H., *Scripta Mater.*, **35**, (1996), 1435.
7. Chia W.J., Chang Y.W., *Intermetallics* **3**, (1995), 505.
8. Takasugi T., Izumi O., *Acta Metall.* **34**, (1996), 607.
9. Klein O., Nagpal P., Baker J., *Mat. Res. Soc. Symp. Proc. Vol 288*, Mater. Res. Soc. (1993), 935.
10. Pike L.M., Liu C.T., *Scripta Mater.* **38**, (1998), 1475.
11. Banerjee P., Balasubramanian R., *Bull. Mater. Sci.*, **30**, (1997), 713.
12. Luu W.C., Wu J.K., *J. Mater. Sci.*, **35**, 2000, 4121.
13. Barcik J., Gierek A., Kupka M., Mikuszewski T., Prandzioch T., Stępień K., *Hutnik i Wiadomości Hutnicze*, **6**, (2001), 214-223.
14. Devanthan M.A., Stachurski Z., *Proc. Roy Soc.*, **A290**, (1960), 90.
15. Barcik J., Stępień K., *Mater. Sci. Eng. A* **334**, (2002), 28-32.
16. Rasek J., *Kinetyka zjawiska wydzielania i rozpuszczania w roztworach stałych α Fe-N/C* Wydawnictwo Uniwersytetu Śląskiego, Katowice 1983.
17. Chiu H., Qiao L., Mao X., *Scripta Mater.* **34**, (1996), 963.
18. Hosoda H., Mizuuchi k., Inoue K., *J. Metals*, **49**, (1997), 56.
19. Yang H., Hanada S., *Scripta Mater.* **32**, (1995), 1719.
20. Zhu Y.F., Liu C.T., Chen C.H., *Scripta Mater.*, **35**, (1996), 1435.
21. Banerjee P., Balasubramanian R., *Scripta Bull. Mater. Sci.*, **20**, (1997), 713.
22. Nishimura C., Liu C.T., *Scripta Mater.*, **35**, (1996), 1441.